DOSIMETRIC INVESTIGATION ON THE DENTAL CONE BEAM COMPUTED TOMOGRAPHY (CBCT) AS AN IMAGING MODALITY FOR PAEDIATRIC CLEFT LIP AND PALATE

NABEEL IBRAHIM ASHOUR

UNIVERSITI SAINS MALAYSIA

2024

DOSIMETRIC INVESTIGATION ON THE DENTAL CONE BEAM COMPUTED TOMOGRAPHY (CBCT) AS AN IMAGING MODALITY FOR PAEDIATRIC CLEFT LIP AND PALATE

by

NABEEL IBRAHIM ASHOUR

Thesis submitted in fulfilment of the requirements for the degree of Doctor of Philosophy

March 2024

ACKNOWLEDGEMENT

In the name of Allah, the Most Gracious and Most Merciful.

Alhamdulillah, all praises are due to Allah SWT for granting me the strength to complete this research. I would like to express my sincere appreciation to the School of Physics at USM for providing me with the opportunity to embark on this research journey.

A special appreciation and heartfelt thanks go to my supervisor, Dr. Nurul Hashikin Ab. Aziz, for her unwavering guidance and constant support. Her dedication and motivation in providing research guidance have been instrumental in the successful completion of this research. I am deeply grateful to my co-supervisors, Dr. Mohd Zahri Abdul Aziz and Dr. Nik Noor Ashikin Nik Ab Razak, who have consistently and convincingly offered me intellectual support, engaged in stimulating discussions, and contributed creative ideas over the years. I also extend my thanks for their outstanding hospitality and persistent assistance.

I would like to extend my gratitude to the entire staff of the School of Physics, the School of Health Sciences, and the Advanced Medical and Dental Institute at USM for their technical assistance and valuable contributions to my work. Their unwavering support and timely advice have been instrumental in my research endeavours. A special acknowledgment goes to all my academic fellows for their continuous support throughout my studies.

Lastly, but by no means least, I extend my heartfelt thanks to fellow researchers and staff from various institutes for their assistance and support, as well as my family and all those who indirectly contributed to the successful completion of this research project.

TABLE OF CONTENTS

| ACK | NOWL | EDGEMEN | NTT | ii |
|------|---------|--------------|---------------------------------------|-------|
| TABL | E OF (| CONTENT | S | iii |
| LIST | OF TA | BLES | | viii |
| LIST | OF FIG | GURES | | X |
| LIST | OF SY | MBOLS AN | ND ABBREVIATIONS | xvii |
| ABST | RAK | ••••• | | xxi |
| ABST | RACT | ••••• | | xxiii |
| CHAI | PTER 1 | INTRODU | UCTION | 1 |
| 1.1 | Backg | round | | 1 |
| 1.2 | Proble | m Statemen | ıt | 3 |
| 1.3 | Aim & | 2 Objective | of Research | 4 |
| 1.4 | Scope | of Study | | 5 |
| 1.5 | Signif | icance of St | udy | 7 |
| 1.6 | Outlin | e of Thesis. | | 7 |
| CHAI | PTER 2 | LITERAT | TURE REVIEW | 9 |
| 2.1 | Cleft I | Lip and Pala | te | 9 |
| | 2.1.1 | Type of Cl | _P | 9 |
| | | 2.1.1(a) | Unilateral and bilateral cleft lip | 9 |
| | | 2.1.1(b) | Cleft palate | 10 |
| | | 2.1.1(c) | CLP combination | 11 |
| | 2.1.2 | Epidemiol | ogy of CLP | 12 |
| | 2.1.3 | Treatment | of CLP | 13 |
| 2.2 | Imagii | ng Modalitie | es for CLP | 14 |
| | 2.2.1 | Overview | of Imaging Modalities | 15 |
| | 2.2.2 | Advantage | es and Disadvantages of Each Modality | 16 |

| 2.3 | Dose | Limit and R | adiation Risks | 18 |
|-----|--------|-------------|--|----|
| 2.4 | Previo | ous Studies | on Dental CBCT | 19 |
| | 2.4.1 | Overview | of Studies | 20 |
| | 2.4.2 | Strengths | and Limitations of Previous Studies | 25 |
| 2.5 | Physic | cal Phanton | ıs | 26 |
| | 2.5.1 | History of | Paediatric Physical Phantoms | 27 |
| | 2.5.2 | Application | ons of Paediatric Physical Phantoms | 27 |
| | 2.5.3 | Current R | esearch in Paediatric Physical Phantoms | 29 |
| 2.6 | Monte | e Carlo and | Voxel Phantom | 33 |
| СНА | PTER 3 | 3 MATERI | ALS AND METHODS | 40 |
| 3.1 | Introd | uction | | 40 |
| 3.2 | | _ | a Paediatric Head and Neck MIRD Model for MC | 41 |
| | 3.2.1 | Modificat | ion of Paediatric MIRD-5 Phantoms | 41 |
| | 3.2.2 | Cone Bea | m Computed Tomography (CBCT) Specifications | 43 |
| | 3.2.3 | Monte Ca | rlo Simulation Setup | 44 |
| | | 3.2.3(a) | X-ray source setup | 44 |
| | | 3.2.3(b) | Tube loading (mAs) and field of view (FOV) setup | 47 |
| | 3.2.4 | Organ Do | ses Estimation by Geant4 | 48 |
| 3.3 | | _ | a Paediatric Head and Neck Voxel Model for MC | 50 |
| | 3.3.1 | Preparation | on of Paediatric ICRP Voxel Phantoms | 51 |
| | | 3.3.1(a) | Selection of images database | 51 |
| | | 3.3.1(b) | Transformation of the binary data into voxel images. | 53 |
| | | 3.3.1(c) | The 3DSlicer segmentation process | 55 |
| | 3.3.2 | CBCT Sp | ecifications and Exposure Parameters Selection | 58 |
| | 3.3.3 | Monte Ca | rlo GATE Simulation | 59 |

| | | 3.3.3(a) | Phantom selection | 59 |
|-----|-------|--------------|--|----|
| | | 3.3.3(b) | X-ray spectrum generation | 59 |
| | | 3.3.3(c) | GATE simulation setup | 59 |
| | | | 3.3.3(c)(i) Placement of the ICRP voxel phantom | 60 |
| | | | 3.3.3(c)(ii) X-ray beam setup | 61 |
| | | | 3.3.3(c)(iii) Beam collimation | 62 |
| | | | 3.3.3(c)(iv) Beam rotation | 63 |
| | | | 3.3.3(c)(v) Dose measurement setup | 64 |
| | 3.3.4 | Organ Do | ses Estimation by GATE Simulation | 65 |
| 3.4 | 3D Pr | inting of Ph | antom Moulds | 66 |
| | 3.4.1 | Skull Segr | mentation | 66 |
| | 3.4.2 | The Proce | ss of Head Segmentation | 67 |
| | 3.4.3 | Slice of Sl | kull and Outer Head Development | 69 |
| | 3.4.4 | Printing th | ne Mould Using 3D Printer | 72 |
| 3.5 | Devel | opment of I | Physical Paediatric Phantom Materials | 77 |
| | 3.5.1 | | of Tissue Equivalent Materials for Newborn and 5- Phantoms | 77 |
| | | 3.5.1(a) | Equivalent substitute-soft tissue for newborn | 78 |
| | | 3.5.1(b) | Equivalent substitute-bone tissue for newborn | 78 |
| | | 3.5.1(c) | Equivalent substitutes-soft tissue and bone tissue for 5-year-old | 79 |
| | 3.5.2 | Fabricatio | n of Phantom's Materials | 79 |
| | 3.5.3 | Radiologi | cal Properties of Tissue Equivalent Materials | 80 |
| | | 3.5.3(a) | Density of sample measurement | 80 |
| | | 3.5.3(b) | Effective atomic number, Z _{eff} | 81 |
| | | 3.5.3(c) | CT number and electron density (ED) | 82 |
| | | 3.5.3(d) | Linear attenuation coefficient (<i>µtissue</i>) based on CT number | 83 |

| | | 3.5.3(e) Mass attenuation coefficient (μ/ρ) | 83 |
|-----|--|---|--------------------------|
| | 3.5.4 | Comparison of USM TE Substitutes to Other Reference Materials | 84 |
| 3.6 | Const | ruction of Head and Neck Physical Paediatric Models | 85 |
| | 3.6.1 | Production of Reciprocal Moulds | 85 |
| | 3.6.2 | Production of Bone Tissue Slices | 87 |
| | 3.6.3 | Production of Soft Tissue Slices and Phantom Assembly | 89 |
| 3.7 | Assess | sment of TLD Properties and Calibration Examination | 91 |
| | 3.7.1 | Sensitivity and Linearity Test | 91 |
| | 3.7.2 | Reproducibility Test | 94 |
| | 3.7.3 | TLD Calibration | 94 |
| | 3.7.4 | Dosimeter Positioning | 98 |
| 3.8 | Organ | Dose Estimation from Dental CBCT and Image Quality | 99 |
| 3.9 | Organ | Doses Estimation by CT Scan and Image Quality | 102 |
| СНА | PTER 4 | RESULTS AND DISCUSSION | 103 |
| 4.1 | Organ | Doses Estimation by Geant4 Simulation | 103 |
| 4.2 | | | |
| | Organ | Doses Estimation by GATE Simulation | 108 |
| 4.3 | _ | Doses Estimation by GATE Simulationlogical Properties of Tissue Equivalent Materials | |
| 4.3 | _ | · | 112 |
| 4.3 | Radio | logical Properties of Tissue Equivalent Materials | 112 112 |
| 4.3 | Radio 4.3.1 | logical Properties of Tissue Equivalent Materials Analysis on Density and Effective Atomic Number | 112 112 115 |
| 4.3 | Radio 4.3.1 4.3.2 | Analysis on Density and Effective Atomic Number Analyses on CT Number and Electron Density (ED) | 112 112 115 117 |
| 4.3 | Radio 4.3.1 4.3.2 4.3.3 4.3.4 | Analysis on Density and Effective Atomic Number | 112 113 115 117 |
| | Radio 4.3.1 4.3.2 4.3.3 4.3.4 | Analysis on Density and Effective Atomic Number | 112 115 117 122 127 |
| | Radio 4.3.1 4.3.2 4.3.3 4.3.4 Assess | Analysis on Density and Effective Atomic Number Analyses on CT Number and Electron Density (ED) Mass Attenuation Coefficient Analysis Comparison of USM TE Substitutes to Other Reference Materials sment of TLD Properties and Calibration Examination | 112 115 117 122 127 |
| | Radio 4.3.1 4.3.2 4.3.3 4.3.4 Assess 4.4.1 | Analysis on Density and Effective Atomic Number | 112 115 117 122 127 129 |

| LIST | OF PUBLICATIONS | |
|------|--|-----|
| REFE | RENCES | 165 |
| 5.2 | Future Recommendations | 164 |
| 5.1 | Conclusion | 161 |
| СНАН | PTER 5 CONCLUSION AND FUTURE RECOMMENDATIONS | 161 |
| | 4.7.1 Comparative Analysis of CBCT and CT Scans Protocols | 158 |
| 4.7 | Organ Doses Estimation from CT scan and Image Quality | 149 |
| 4.6 | Comparative Analysis: CBCT Dose Assessment Comparison with Geant4 and GATE Simulations | |

LIST OF TABLES

| | | Page |
|-----------|--|------|
| Table 2.1 | Quantifying Radiation Risks: Incorporating Detriment- Adjusted Nominal Risk Coefficients for Stochastic Effects | 19 |
| Table 2.2 | The risk estimates were adapted from the ICRP 1990 publication and are based on the multiplicative risk projection model. | 19 |
| Table 2.3 | Effective dose range of dental CBCT for adult phantoms: comparing large >15 cm height, medium 10 -15 cm height, and small < 10 cm height field of view exposures. | 20 |
| Table 2.4 | Effective dose range of dental CBCT for paediatric phantoms: comparing large >15 cm height, medium 10 -15 cm height, and small < 10 cm height field of view exposures. | 21 |
| Table 2.5 | Effective dose comparison among conventional dental devices | 24 |
| Table 2.6 | Details of each review articles regarding the 3D printing phantoms, medical diagnostic scanners. | 31 |
| Table 3.1 | The reference values of organ mass, volume, density, and head circumference for newborn male [201, 215-219] | 42 |
| Table 3.2 | The reference values for organ mass, volume, density, and head circumference for 5-year-old male [201, 215-219] | 43 |
| Table 3.3 | The technical specifications of the Planmeca Promax 3D classic CBCT. | 43 |
| Table 3.4 | Exposure parameters and indications of acquisition protocol | 48 |
| Table 3.5 | Main characteristics of the reference paediatric computational phantoms. | 53 |
| Table 3.6 | Material compositions of tissue- equivalent substitutes | 77 |
| Table 3.7 | Dosimeter placement locations in the slices of the head and neck of a physical newborn phantom. | 99 |
| Table 3.8 | Dosimeter placement locations in the slices of the head and neck of a physical 5-year-old phantom | 99 |
| Table 4.1 | Absorbed organ doses (mGy) for various exposure parameters in the head and neck of the newborn MIRD phantom | 104 |

| Table 4.2 | Absorbed organ doses (mGy) for various exposure parameters in the head and neck of the 5-year-old MIRD phantom |
|------------|--|
| Table 4.3 | Absorbed organ doses (mGy) for various exposure parameters in the head and neck of the newborn ICRP voxel phantom 109 |
| Table 4.4 | Absorbed organ doses (mGy) for various exposure parameters in the head and neck of the 5-year-old ICRP voxel phantom 109 |
| Table 4.5 | Elemental composition and effective atomic numbers of USM newborn equivalent tissue and corresponding ORNL newborn reference tissue compositions |
| Table 4.6 | Elemental composition and effective atomic numbers of USM equivalent tissues for a 5-year-old phantom and corresponding reference tissue compositions from the ORNL model at a similar age |
| Table 4.7 | The mean CT number and the electron density for each plug phantom at 52 keV |
| Table 4.8 | Absorbed organ doses (mGy) for various exposure parameters by CBCT in the head and neck of the newborn physical phantom. |
| Table 4.9 | Absorbed organ doses (mGy) for various exposure parameters by CBCT in the head and neck of the 5-year-old physical phantom |
| Table 4.10 | CBCT image measurements of newborn and 5-year-old phantoms |
| Table 4.11 | CT image parameters of newborn and 5-year-old phantoms 156 |
| Table 4.12 | Comparative analysis of CBCT and CT scans protocols results |

LIST OF FIGURES

| | | Page |
|------------|--|------|
| Figure 2.1 | Illustration of Unilateral and Bilateral Cleft Lip Variants (Adapted from [31]). | 9 |
| Figure 2.2 | Illustration of cleft palate (Adapted from [31]) | 10 |
| Figure 2.3 | Illustration of both cleft lip and cleft palate (Adapted from [31]) | 11 |
| Figure 2.4 | Average contribution of organ doses to effective dose calculations for CBCT. | 22 |
| Figure 2.5 | Percent fraction of radiation dose for the different tissues in the head derived from the MC-GPU simulation of the human head exposed to cone-beam computed tomography | 23 |
| Figure 2.6 | ORNL stylized phantom series: (a) External Views of Computational Hermaphrodite MIRD-5 Phantom, and (b) Stylized Phantom - Various Ages, (adapted from [190]) | 36 |
| Figure 2.7 | International Commission on Radiological Protection series of reference paediatric voxel-based computational phantoms (adapted from [209]). | 38 |
| Figure 2.8 | Reference size computational human phantoms (hybrid) ranging from newborn to adults (adapted from [212]) | 39 |
| Figure 3.1 | Flowchart of the analyses performed in this study | 40 |
| Figure 3.2 | The modified head and neck phantoms for (a) newborn, and (b) 5-year-old. | 42 |
| Figure 3.3 | Geant4 macro lines in (primary. mac) file used to define the radiation source /rotation. | 45 |
| Figure 3.4 | The full-rotation CBCT geometry. The lateral and superior views of newborn simulation are illustrated in (a) and (b), respectively, while the lateral and superior views of the 5-year-old simulation are illustrated in (c) and (d), respectively | 46 |
| Figure 3.5 | The X- ray spectra used in the Geant4 simulation to simulate the beam generated by the Planmeca Promax 3D classic | 47 |
| Figure 3.6 | Visualising the cone-beam x-ray simulated using Geant4: (a) frontal and (b) lateral views for MIRD newborn head phantom. | 49 |

| Figure 3.7 | Visualising the cone-beam x-ray simulated using Geant4: (a) lateral and (b) frontal views for MIRD 5-year-old head phantom. | 49 |
|-------------|---|----|
| Figure 3.8 | The process of importing binary data to (X) MedCon: (a) open file, (b) open RAW file (interactive), (c) input header information and (d) input image information steps. | 54 |
| Figure 3.9 | Preliminary images produced via binary data conversion by (X)MedCon. | 54 |
| Figure 3.10 | The process of saving the images: (a) save as (select Analyze), (b) save file, and (c) final file name saved as (binary.hdr) | 55 |
| Figure 3.11 | Transferring an image file from (X) Medcon to 3DSlicer | 56 |
| Figure 3.12 | The conversion of label map model process: (a) Selecting active volume, (b) dimensions and spacing image input information and (c) conversion to label map | 57 |
| Figure 3.13 | The processes of segmentation and saving the files: (a) convert label map to segmentation node, (b) (1-140) nodes segmented, and (c) save data as Meta image (.mhd). | 58 |
| Figure 3.14 | ICRP paediatric voxel phantoms at the centre of GATE simulation world: (a) newborn phantom and (b) 5-year-old phantom. | 60 |
| Figure 3.15 | Macro lines code in (patient.mac) file used to setup a voxel phantom position in GATE simulation | 61 |
| Figure 3.16 | Energy spectrum file | 62 |
| Figure 3.17 | GATE simulation of cone beam of X-ray lateral views: (a) newborn voxel phantom, and (b) 5-year-old voxel phantom | 63 |
| Figure 3.18 | GATE macro lines commands in (Beam.mac) file used to define X-ray rotation. | 63 |
| Figure 3.19 | The DoseActor file code in GATE simulation. | 65 |
| Figure 3.20 | The process of left: the skull segmentation tools, and right: the outcome of the skull segmentation process. | 67 |
| Figure 3.21 | The process of face segmentation by 3DSlicer. | 68 |
| Figure 3.22 | Face segmentation output: (a) before cutting (lateral view) and (b) final face after (frontal view) cutting by scissors | 69 |
| Figure 3.23 | Slice of skull and outer head development: (a) segmentation editor by ruler tool to create box covering skull; (b) a box | |

| | and (d) outer head layers with 1 cm thickness; and (d) outer head layers with 1 cm thickness | 70 |
|-------------|---|----|
| Figure 3.24 | 3D models as STL files: (a) export segment volume to 3D models and saved as STL files for (a) outer head layers and (b) skull layers. | 71 |
| Figure 3.25 | Ultimaker 2+extended 3D printer | 73 |
| Figure 3.26 | Whole skull slices with neck vertebrae before printing | 73 |
| Figure 3.27 | Skull and outer head before printing: (a) one layer includes the skull and outer head; (b) the outer head layer is part only; and (c) the skull layer is part only. | 74 |
| Figure 3.28 | 3D printing mould layers of the skull, outer head, and neck of a newborn male. | 75 |
| Figure 3.29 | 3D printing mould layers of the skull, outer head, and neck of a 5-year-old male. | 76 |
| Figure 3.30 | Methodology and equipment for manufacturing equivalent substitutes of the soft and bone tissues. | 80 |
| Figure 3.31 | Blue silicone rubber moulds used to produce the reciprocal moulds for 5-year-old phantom slices. | 86 |
| Figure 3.32 | The reciprocal moulds after removing the PLA mould for 5-year-old phantom slices. | 86 |
| Figure 3.33 | The reciprocal moulds filled with the bone equivalent tissue | 88 |
| Figure 3.34 | Placement of 5-year-old bone equivalent tissues within the outer head mould slices. | 88 |
| Figure 3.35 | Placement of newborn bone equivalent tissues within the outer head mould slices. | 89 |
| Figure 3.36 | The final step of a newborn slice formation, soft and bone equivalent tissue. | 90 |
| Figure 3.37 | The final step of a 5-year-old slice formation, soft and bone equivalent tissue. | 90 |
| Figure 3.38 | Different side views of the assembled paediatric head and neck phantom slices – a) newborn with CLP and b) 5-Year-old with CLP | 91 |
| Figure 3.39 | Linearity test setup | 93 |
| Figure 3.40 | Setup of TLD calibration. | |
| | | |

| Figure 3.41 | Setup of head phantoms: Left - newborn, Right - 5-year-old, for CBCT imaging with diverse exposure parameters |
|-------------|---|
| Figure 4.1 | Effective organ doses (mSv) with various exposure parameters in the head and neck of the newborn and 5-year-old MIRD phantoms |
| Figure 4.2 | Average contribution of organ doses to effective dose calculations for newborn- MIRD phantom by Geant4- CBCT simulation |
| Figure 4.3 | Average contribution of organ doses to effective dose calculations for 5-year-old - MIRD phantom by Geant4-CBCT simulation |
| Figure 4.4 | Effective organ doses (mSv) with various exposure parameters in the head and neck of the newborn and 5-year-old ICRP phantoms |
| Figure 4.5 | Average contribution of organ doses to effective dose calculations for newborn- ICRP phantom by GATE- CBCT simulation |
| Figure 4.6 | Average contribution of organ doses to effective dose calculations for 5-year-old - ICRP phantom by GATE- CBCT simulation. 112 |
| Figure 4.7 | Variation of CT Numbers with Diagnostic Photon Energy Range (47 to 66 keV) for Different USM Tissue-Equivalent Substitutes |
| Figure 4.8 | Electron density calibration curve against the CT number at tube voltage 52 keV for ^a Water, ^b Liver, ^c Muscle, ^d Bone 200, ^e Bone 800, and ^f Bone 1250 |
| Figure 4.9 | The ratio of mass attenuation coefficient μ/ρ to their corresponding reference tissues for the newborn phantom model as a function of diagnostic energy. |
| Figure 4.10 | The ratio of mass - energy attenuation coefficient μen/ρ to their corresponding reference tissues for the newborn phantom model as a function of diagnostic energy |
| Figure 4.11 | The ratio of mass attenuation coefficient μ/ρ for the ESST and ESBT equivalent tissues to their corresponding reference attenuation values for ORNL (5-year-old model) as a function of diagnostic energy. |
| Figure 4.12 | The ratio of mass energy attenuation coefficient μen/ρ for the ESST and ESBT equivalent tissues to their corresponding reference attenuation values for ORNL (5-year-old model) as a function of diagnostic energy. |

| Figure 4.13 | Relationship between ratios of μ/ρ and μ en/ ρ for ESST-NB and Acrylic and their corresponding reference values of ORNL newborn model with respect to diagnostic energy |
|-------------|--|
| Figure 4.14 | Relationship between ratios of μ/ρ and $\mu en/\rho$ for ESBT-NB and Aluminium and their corresponding reference values of ORNL newborn model with respect to diagnostic energy 123 |
| Figure 4.15 | Ratios of μ/ρ and $\mu en/\rho$ for ESST, MS11, and Acrylic to their corresponding reference values of ORNL (5-year-old model) as a function of diagnostic energy. |
| Figure 4.16 | Variation of ratios of μ/ρ for ESBT, IB1, SB5, weighted combination of IB1 and SB5, and Aluminium relative to corresponding reference values of ORNL (5-Year-Old) with respect to photon energy |
| Figure 4.17 | Variation of ratios of $\mu en/\rho$ for ESBT, IB1, SB5, weighted combination of IB1 and SB5, and Aluminium relative to corresponding reference values of ORNL (5-Year-Old) with respect to photon energy. |
| Figure 4.18 | Sensitivity test for all TLDs |
| Figure 4.19 | Linearity test for TLD (G1) |
| Figure 4.20 | The percentage of coefficient of variation for all TLDs |
| Figure 4.21 | Effective organ doses (mSv) with various exposure parameters in the head and neck of the newborn and 5-year-old physical phantoms |
| Figure 4.22 | Average contribution of organ doses to effective dose calculations for newborn- physical phantom by CBCT |
| Figure 4.23 | Average contribution of organ doses to effective dose calculations for 5-year-old- physical phantom by CBCT |
| Figure 4.24 | Cleft CBCT images for newborn head phantom at low resolution protocol: 90 kVp , 7.184 mAs , $68 \times 68 \text{ mm}^2$ (FOV). |
| Figure 4.25 | Cleft CBCT images for newborn head phantom at low resolution protocol: 90 kVp, 19 mAs, 68×68 mm ² (FOV) 139 |
| Figure 4.26 | Cleft CBCT images for newborn head phantom at low resolution protocol: 90 kVp, 36.996 mAs, 68 × 68 mm ² (FOV) |
| Figure 4.27 | Cleft CBCT images for newborn head phantom at normal resolution protocol: 90 kVp, 38.325 mAs, 68 × 68 mm ² (FOV) |
| | |

| Figure 4.28 | Cleft CBCT images for newborn head phantom at high resolution protocol: 90 kVp, 110.835 mAs, 68 × 68 mm ² (FOV) |
|-------------|---|
| Figure 4.29 | Cleft CBCT images for 5-year-old head phantom at low resolution protocol: 90 kVp, 7.184 mAs, 68 × 68 mm ² (FOV). |
| Figure 4.30 | Cleft CBCT images for 5-year-old head phantom at low resolution protocol: 90 kVp, 19 mAs, 68×68 mm ² (FOV) 141 |
| Figure 4.31 | Cleft CBCT images for 5-year-old head phantom at low resolution protocol: 90 kVp, 36.996 mAs, 68 × 68 mm ² (FOV) |
| Figure 4.32 | Cleft CBCT images for 5-year-old head phantom at normal resolution protocol: 90 kVp, 38.325 mAs, 68 × 68 mm ² (FOV) |
| Figure 4.33 | Cleft CBCT images for 5-year-old head phantom at high resolution protocol: 90 kVp, 110.835 mAs, 68 × 68 mm ² (FOV) |
| Figure 4.34 | A comparative analysis of absorbed dose in the head and neck OARs: Monte Carlo simulation (Geant4 and GATE) and experimental assessment using a newborn phantom for CBCT exposure at 90 kVp and 19 mAs |
| Figure 4.35 | A comparative analysis of absorbed dose in the head and neck OARs: Monte Carlo simulation (Geant4 and GATE) and experimental assessment using a 5-year-old phantom for CBCT exposure at 90 kVp and 19 mAs |
| Figure 4.36 | Influence of increased exposure parameters on effective dose in newborn and 5-year-old phantoms: validation through Geant4, GATE, and experimental CBCT approaches |
| Figure 4.37 | A comparative analysis of absorbed doses (mGy) for organs at risk (OARs) was conducted in newborn and 5-year-old phantoms under CT scan exposure conditions |
| Figure 4.38 | Effective organ doses (mSv) exposed to CT scan protocols in the head and neck of newborn and 5-Year-Old physical phantoms |
| Figure 4.39 | Average contribution of organ doses to effective dose calculations for newborn- physical phantom by CT scan protocol (Brain baby 0-2 years) |
| Figure 4.40 | Average contribution of organ doses to effective dose calculations for 5-year-old- physical phantom by CT scan protocol and (Brain child 3-5 years) |

| Figure 4.41 | CT images for: a) cleft palate for a newborn head phantom at |
|-------------|---|
| | Brain baby 0-2 year protocol, and b) cleft palate for a 5-year- |
| | old head phantom at brain child 3-5 years protocol, 150 x 68 |
| | mm ² (FOV) |

LIST OF SYMBOLS AND ABBREVIATIONS

% Percentage

°C Degree in Celsius

 $\mu \rho$ Mass attenuation coefficient

 μ_{en}/ρ Mass-energy attenuation coefficient

μC Micro-Coulomb

 μ_{tissue} Tissue linear attenuation coefficient

ρ Density

A Mass number

C Carbon

Ca Calcium

CHN Carbon, hydrogen, nitrogen

Cl Chlorine

cm Centimetre

g Gram

g·cm³ Gram per centimetre cubic

H Hydrogen

h Hour

K potassium

keV Kilo electron Volt

kg kilogram

kVp kilovolt peak

Mg Magnesium

min Minute

N Nitrogen

Na Sodium

O Oxygen

s Second

Z Atomic number

2D 2-Dimensional

3D 3-Dimensional

AIDR 3D Adaptive Iterative Dose Reduction 3D

AMDI Advanced Medical and Dental Institute

CBCT Cone beam computed tomography

CF Calibration factor

CLP Cleft lip and palate

CNR Contras- to-Noise Ratio

CT Computed tomography

DICOM Digital Imaging and Communication in Medicine

D_{mean} Mean dose

ECC Element Correction Coefficient

ED Effective dose

EDX Energy dispersive X-ray

EGSnrc Electron Gamma Shower by National Research Council

ESBT Equivalent substitute-bone tissue

ESBT-NB Equivalent substitute-bone tissue for the newborn

ESST Equivalent substitute-soft tissue

ESST-NB Equivalent substitute-soft tissue for the newborn

GATE Geant4 Application for Tomographic Emission

GEANT4 Geometry and Tracking

GPS General Particle Source

H_T Equivalent dose

HU Hounsfield Unit

IC Ionisation chamber

ICRP International Commissioning of Radiation Protection

ICRU International Commissioning of Radiation Units and Measurement

L Left

LiF Lithium fluoride

mAs Milli Ampere-second

MC Monte Carlo

MeV Mega electron Volt

mGy Milli-Gray

MIRD Medical Internal Radiation Dose

mL Millilitre

MRI Magnetic resonance imaging

nC Nano-Coulomb

NIST National of Institute Standard Technology

OAR Organ at risk

ORNL Oak Ridge National Laboratory

PLA Polylactic acid

PMMA Polymethylmethacrylate

QA Quality Assurance

R Right

ROI Regions of interest

SD Standard deviation

TE Tissue equivalent

TLD Thermo luminescent dosimeter

UF University of Florida

USM Universiti Sains Malaysia

W_i Electron fraction

W_T Weighting tissue factor

W_R Weighting radiation factor

XCOM Photon Cross Sections Database

Z_{eff} Effective atomic number

PENYIASATAN DOSIMETRIK TERHADAP TOMOGRAFI BERKOMPUTER ALUR KON PERGIGIAN (CBCT) SEBAGAI MODALITI PENGIMEJAN UNTUK BIBIR DAN LELANGIT SUMBING PEDIATRIK

ABSTRAK

Kemajuan pengimejan perubatan telah meningkatkan perancangan diagnostik dan rawatan dengan ketara untuk pelbagai keadaan perubatan, termasuk bibir sumbing dan lelangit (CLP). Walau bagaimanapun, kebimbangan mengenai pendedahan sinaran mengion dalam pesakit kanak-kanak, terutamanya mereka yang berumur di bawah 6 tahun, telah membawa kepada penyiasatan terhadap alternatif pengimejan yang lebih selamat. Kajian ini memberi tumpuan kepada penggunaan Alur kon dental tomografi berkomputer (CBCT) sebagai modaliti pengimejan untuk pesakit CLP pediatrik, bertujuan untuk menilai keselamatan dan kebolehlaksanaannya melalui siasatan dosimetrik yang komprehensif. Untuk mencapai objektif ini, fantom kepala dan leher setara tisu (TE) terperinci yang mewakili bayi baru lahir dan 5 tahun telah dicipta menggunakan teknik pembuatan termaju, terutamanya percetakan 3D. Simulasi Monte Carlo digunakan untuk pemodelan interaksi sinaran, dan perbandingan antara pengukuran dan simulasi empirikal telah dijalankan menggunakan perisian Geometri dan Penjejakan, Versi 4 (Geant4), dan Aplikasi Geant4 untuk Pembebasan Tomografi (GATE). Dos organ dinilai untuk kedua-dua CBCT dan imbasan tomografi terkira (CT) konvensional. Hasilnya menunjukkan bahawa fantom TE yang dibangunkan dengan tepat mereplikasi ciri anatomi dan radiografi kumpulan umur yang disasarkan. Parameter seperti ketumpatan, nombor atom berkesan, nombor CT, ketumpatan elektron, pekali pengecilan jisim, dan pekali penyerapan tenaga jisim hampir sepadan dengan sistem fantom rujukan. Apabila dibandingkan dengan sampel rujukan Makmal Kebangsaan Oak Ridge (ORNL), penggantian TE yang baru lahir menunjukkan percanggahan dalam julat yang boleh diterima merentas spektrum tenaga. Untuk imbasan CBCT, purata dos Dosimeter Termo-Bercahaya (TLD) untuk fantom yang baru lahir adalah antara 0.019 mSv hingga 1.84 mSv, bergantung pada parameter pendedahan. Begitu juga, untuk fantom 5 tahun, dos berjulat dari 0.011 mSv hingga 0.46 mSv. Sebaliknya, imbasan CT merekodkan dos TLD yang lebih tinggi, dengan dos berkesan 7.92 mSv untuk fantom yang baru lahir dan 10.46 mSv untuk fantom berusia 5 tahun. Anggaran dos organ mencadangkan bahawa walaupun CBCT boleh mentadbir dos yang lebih rendah daripada imbasan CT, terdapat pertukaran antara pengurangan dos sinaran dan kualiti imej. Kajian itu menunjukkan bahawa protokol pendedahan boleh mengurangkan nilai dos sinaran secara berkesan di bawah ambang 16.66 mSv, mengekalkan imej yang bernilai secara diagnostik. Keputusan ini menggariskan potensi CBCT sebagai kaedah pengimejan alternatif yang boleh dilaksanakan untuk campur tangan awal dalam kes CLP pediatrik, yang berpotensi meningkatkan ketepatan perancangan rawatan dan hasil pesakit.

DOSIMETRIC INVESTIGATION ON THE DENTAL CONE BEAM COMPUTED TOMOGRAPHY (CBCT) AS AN IMAGING MODALITY FOR PAEDIATRIC CLEFT LIP AND PALATE

ABSTRACT

Medical imaging advancements have significantly improved diagnostic and treatment planning for various medical conditions, including cleft lip and palate (CLP). However, concerns about ionising radiation exposure in paediatric patients, especially those under 6 years old, have led to investigations into safer imaging alternatives. This study focuses on using dental cone beam computed tomography (CBCT) as an imaging modality for paediatric CLP patients, aiming to assess its safety and feasibility through a comprehensive dosimetric inquiry. To achieve this objective, detailed tissueequivalent (TE) head and neck phantoms representing newborn and 5-year-olds were created using advanced manufacturing techniques, particularly 3D printing. Monte Carlo simulations were employed for radiation interaction modelling, and comparisons between empirical measurements and simulations were conducted using Geometry and Tracking, Version 4 (Geant4), and Geant4 Application for Tomographic Emission (GATE) software. Organ doses were evaluated for both CBCT and conventional computed tomography (CT) scans. The outcomes indicated that the developed TE phantoms accurately replicated the anatomical and radiographic features of the targeted age groups. Parameters such as density, effective atomic number, CT numbers, electron densities, mass attenuation coefficients, and mass energy absorption coefficients closely matched those of the reference phantom system. When compared with the Oak Ridge National Laboratory (ORNL) reference samples, the newborn TE substitutions demonstrated discrepancies within acceptable ranges across an energy

spectrum. For the CBCT scans, the average Thermal-Luminescent Dosimeter (TLD) doses for the newborn phantom ranged from 0.019 mSv to 1.84 mSv, depending on exposure parameters. Similarly, for the 5-year-old phantom, doses ranged from 0.011 mSv to 0.46 mSv. In contrast, CT scans recorded higher TLD doses, with effective doses of 7.92 mSv for the newborn phantom and 10.46 mSv for the 5-year-old phantom. Estimations of organ doses suggested that while CBCT can administer lower doses than CT scans, there is a trade-off between radiation dose reduction and image quality. The study demonstrated that exposure protocols can effectively decrease radiation dose values below the threshold of 16.66 mSv, maintaining diagnostically valuable images. These results underscore the potential of CBCT as a feasible alternative imaging method for early intervention in paediatric CLP cases, potentially enhancing treatment planning precision and patient outcomes.

CHAPTER 1

INTRODUCTION

1.1 Background

The second most common birth defect in the United States is cleft lip with or without cleft palate, affecting 1 in every 940 births and resulting in 4,437 cases every year [1]. Reported prevalence incidence extent from 7.75 to 10.63 per 10,000 live births [1, 2]. The case of cleft lip and palate (CLP) varies particularly among different racial groups. In the United States, 1 in 500 incidences involved the Asians and Native Americans, 1 in 1,000 incidences involved the Caucasian Americans, and approximately 1 in 2,400 to 2,500 incidences in the African Americans [3-6].

In Malaysia, majority of patients with CLP are of Malay ethnic group (88.6 %), followed by Chinese (3.9 %), Indians (2.5 %) and others (0.2 %). CLP is one of the major causes of increased infant deathrate and poor quality of life worldwide. CLP patients in developing countries face larger problems, especially due to absence of access to standard healthcare. Patients with CLP, if left untreated, may experience poor nutrition, and speech difficulties. In addition, the risk of hearing loss and delayed midface growth are also present [7, 8].

The diagnosis of cleft lip with or without cleft palate (CLP) presents significant challenges due to its intricate etiological factors and the wide array of associated symptoms. In this complex scenario, diagnostic imaging emerges as a crucial tool in facilitating accurate diagnosis. Various diagnostic techniques have been employed for CLP, including panoramic radiography, transcranial radiography, CT scan, and magnetic resonance imaging (MRI) [9]. Historically, conventional radiography guided treatment decisions, but the trend has shifted towards more precise diagnoses using

specialized imaging methods like CT, and MRI [10, 11], offering the potential for improved accuracy in diagnosis and treatment planning.

However, the selection of appropriate imaging modalities may be influenced by factors such as cost, time, and radiation exposure, prompting the need for imaging guidelines. Among the available options, CBCT and CT stand out as suitable choices for assessing changes related to sclerosis, flattening, erosion, and osteophyte formation [12]. The superior advantages of CBCT, including lower radiation dose and isotropic resolution, position it as a preferable choice over CT for evaluating hard tissue structures [13]. This is particularly significant when distinguishing between hard and soft tissue concerns based on a comprehensive clinical assessment of CLP patients. Therefore, an informed decision can be made to opt for CBCT (or CT) or MRI for a targeted imaging work-up.

Recent strides in prenatal imaging have enabled the in-utero diagnosis of CLP and associated deformities [14, 15], contributing to earlier intervention. While clinical diagnosis remains central postnatally, imaging assumes a pivotal role in identifying related anomalies, aiding surgical planning, and managing minor deformities. While general radiography lacks utility in diagnosing CLP, panoramic and dental radiographs are employed to identify concomitant dental issues [16].

MRI emerges as valuable in confirming and characterizing CLP, particularly when used alongside ultrasonography for prenatal assessment. However, postnatally, MRI typically doesn't play a direct role in describing the cleft itself [14], although coronal MRI images offer better depiction of the condition, and sagittal MR images can also reveal CLP [17]. CT imaging, on the other hand, is frequently utilised prior to corrective procedures for dentofacial deformities, particularly for showcasing bone

and dental anatomy [18]. Enhanced diagnostic accuracy is facilitated through multiplanar reconstructions of helical CT images, aided by bone and soft-tissue algorithms, contributing to the detailed description of anatomic abnormalities.

Considering the wide spectrum of diagnostic techniques, CBCT emerges as a frontrunner due to its distinct advantages in terms of radiation dose and resolution for hard tissue assessment. Hence, CBCT is recommended as the optimal imaging modality for CLP in paediatric patients, providing a comprehensive diagnostic approach that addresses the intricate aspects of this condition.

1.2 Problem Statement

Surgical planning of CLP typically starts when the patient reaches 6 years old [19]. Although CT can be helpful in the 3D reconstruction of the patient's anatomy, it uses ionising radiation in a significantly high dose, thus, has been of major concern for patients younger than 6 years old. Quality of life especially in terms of feeding and speech development are crucial for children at ages younger than 6, hence, earlier treatment is essential to ensure that these skills are not affected. CBCT is one of the recent advancements in CT technology, which has been increasingly used for patients requiring dentofacial treatments. It has been reported that CBCT can provide image quality as good as CT, with significantly lower dose [20]. Thus, this study proposes dental CBCT to be used as an alternative imaging modality for the treatment management of CLP in patients younger than 6 years old, i.e., newborn and 5-year-old males. The key objective of this research is to perform a comprehensive investigation into radiation dose, providing important data on radiation exposure through the fabrication of two sets (newborn and 5-year-old) of anatomically accurate tissue-equivalent head and neck physical phantoms. This data will be used to make informed

decisions on the practicality and safety of using dental CBCT for early intervention in cleft lip and palate cases. This approach is in line with larger endeavours to reduce radiation exposure, particularly in paediatric populations, and optimise CBCT techniques to achieve a balance between diagnostic image quality and radiation amount [21-23]. In addition, the study includes a thorough comparison, evaluating the advantages and disadvantages of dental CBCT in paediatric use in relation to other imaging techniques such as conventional CT or MRI [23, 24]. The research seeks to provide significant insights into the possible benefits and limitations of using oral CBCT for early intervention in CLP patients. The study seeks strategies to increase patient comfort, minimise the need for anaesthesia, and enhance safety during CBCT scans in paediatric patients [25, 26]. This strategy is in line with the overarching objective of resolving patient safety issues and protecting the welfare of young kids with CLP who are having dental CBCT treatments. In summary, this research seeks to tackle the significant obstacles related to concerns about radiation dose, imaging quality, and patient safety when it comes to early intervention for CLP patients who are under 6 years old. The effort intends to use dental CBCT to enhance decisionmaking in paediatric dentofacial treatments.

1.3 Aim & Objective of Research

The aim of this study was to develop paediatric head and neck physical phantoms that can be used to investigate the safety of dental CBCT as the main imaging modality for the purpose of treatment planning for CLP in paediatric patients younger than 6 years old. This can be achieved by fulfilling the following objectives:

- To fabricate two sets (newborn and 5-year-old) of anatomically accurate tissue-equivalent head and neck physical phantoms for radiation dosimetry studies.
- To evaluate the radiation absorbed doses to OARs in the head and neck region following dental CBCT exposures using the fabricated physical phantoms.
- validate the measured absorbed dose obtained from the CBCT exposures using Geant4 and GATE Monte Carlo (MC) simulations and assess the magnitude of radiation risk in paediatric patients.
- iv) Perform a comparative analysis of CBCT and CT scan protocols.

1.4 Scope of Study

The scope of this study encompasses a comprehensive evaluation of radiation doses to organs at risk (OARs) in the head and neck of paediatric patients with cleft lip and palate (CLP) undergoing dental CBCT and conventional CT scans under various exposure parameters. The primary aims of this study are two-fold: firstly, to develop anatomically accurate tissue-equivalent head and neck phantoms for radiation dosimetry studies, and secondly, to assess radiation doses received by OARs during these imaging procedures.

i. Phantom Development: A significant aspect of the study involves the creation of two sets of anatomically accurate tissue-equivalent head and neck phantoms representing newborn and 5-year-old paediatric patients. These phantoms will be constructed using epoxy resin combined with various filler materials. The development of these phantoms allows for accurate radiation dosimetry studies, providing

insights into the radiation doses received by paediatric patients during imaging procedures.

- ii. Utilisation of 3D Printing: The construction of paediatric phantoms involves the utilisation of 3D printing technology to create moulds based on ICRP voxel data. The moulds will be processed using 3DSlicer and (X)Medcon software to achieve high anatomical fidelity in the resulting phantoms.
- iii. Dosimetric Modelling: Paediatric head and neck MIRD-5 and voxel models will be developed for Monte Carlo (MC) dosimetric studies. These models will aid in simulating and predicting absorbed doses to various tissues and organs during imaging procedures.
- iv. Radiation Dose Evaluation: The primary focus is to quantify the radiation doses to organs at risk (OARs) in the head and neck region of paediatric patients with CLP undergoing dental CBCT and CT scans. The study encompasses variations in exposure parameters to understand their impact on dose distribution. The absorbed doses to OARs will be measured using thermoluminescence detectors (TLDs) placed within the anatomically accurate phantoms during exposure. These measured doses will then be compared with doses simulated using MIRD-5 and ICRP voxel phantoms. Additionally, a comparison will be made with absorbed doses resulting from standard CT scan protocols, assessing the potential radiation risks associated with the procedures.

1.5 Significance of Study

This study will provide a database of radiation absorbed doses to the head and neck organs of newborn and 5-year-old patients from dental CBCT exposure during the planning of CLP treatment. These organs at risk (OARs) include the brain, brainstem, cochlea, eyeballs, eye lens, parotid glands, optic chiasm, optic nerve, and thyroid. Dental CBCT exposures representing all the steps involved during the planning of CLP treatment will be performed on two sets of newborn and 5-year-old head and neck phantoms (tissue-equivalent materials that represent the radiation properties similar to actual human tissues), which will be developed and installed using 3D-printed moulds, representing the CLP patients.

Thermoluminescence detectors (TLDs) will be placed inside the OARs during the exposures to record the absorbed doses received by these OARs. The absorbed doses will then be compared with a computer-based simulation based on MIRD-5 and ICRP voxel phantoms, where the recorded absorbed dose will be verified. Additionally, the dose will be compared with the absorbed doses of the standard CT scan protocols recommended for those patients. The dose will then be evaluated in relation to the magnitude of radiation risk.

1.6 Outline of Thesis

There are five chapters in this thesis. Chapter 1 consists of the introduction, which includes the background of the study, the problem statement, the aims and objectives of the research, and the scope and significance of the study. Chapter 2 consists of the literature review, covering theoretical aspects related to cleft lip and palate (types, staging, definition, epidemiology, treatment, and diagnosis), an overview of imaging modalities for paediatric cleft lip and palate, advantages and disadvantages

for each modality, dose limit, and radiation risks, an overview of previous studies on dental CBCT, strengths, and limitations of previous studies, history, application, and current research of paediatric physical phantoms, Monte Carlo method, and voxel phantom. Chapter 3 describes the technical aspects related to the development of paediatric head and neck MIRD models for MC dosimetric study, the development of paediatric head and neck voxel models for MC GATE dosimetric study, the process of 3D printing phantom moulds, the development of physical paediatric phantom materials, construction of head and neck physical paediatric models, assessment of TLD properties and calibration examination, and organ dose estimation by CBCT and CT scan. The results and discussions are reported in Chapter 4. Finally, the study concludes in Chapter 5, along with recommendations to improve this study.

CHAPTER 2

LITERATURE REVIEW

2.1 Cleft Lip and Palate

Cleft lip and palate (CLP) are a common congenital craniofacial anomaly that affects approximately 1 in 700 live births worldwide [27, 28]. The condition arises during foetal development when there is incomplete fusion of the lip and/or palate structures, leading to a range of clinical presentations. The severity and type of cleft vary, encompassing unilateral or bilateral cleft lips, cleft palates, or a combination of both. Proper understanding of the types and staging of cleft lips and palates is crucial for clinicians, surgeons, and researchers alike, as it influences the treatment approach, timing, and outcomes [27-29].

2.1.1 Type of CLP

2.1.1(a) Unilateral and bilateral cleft lip

Cleft lips can be categorized into unilateral (affecting one side of the lip) or bilateral (affecting both sides), as shown in Figure 2.1. The prevalence of these types may vary among populations [29, 30].



Unilateral cleft lip



Bilateral cleft lip

Figure 2.1 Illustration of Unilateral and Bilateral Cleft Lip Variants (Adapted from [31]).

2.1.1(b) Cleft palate

Cleft palate can occur as an isolated anomaly or in conjunction with cleft lip, as shown in Figure 2.2. It can further be categorized into subtypes, including the complete cleft palate, incomplete cleft palate, and submucous cleft palate, each with its own anatomical characteristics and clinical implications [32-34].

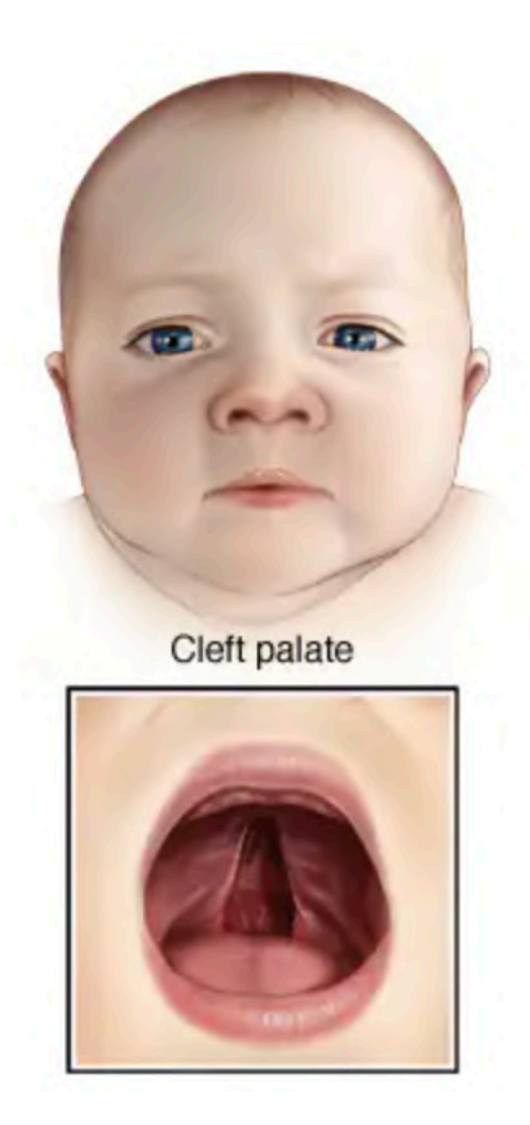


Figure 2.2 Illustration of cleft palate (Adapted from [31]).

2.1.1(c) CLP combination

Some individuals may have both cleft lip and cleft palate, leading to a more complex condition, as shown in Figure 2.3. Understanding the specific combination and the extent of involvement is essential for treatment planning [30, 33].

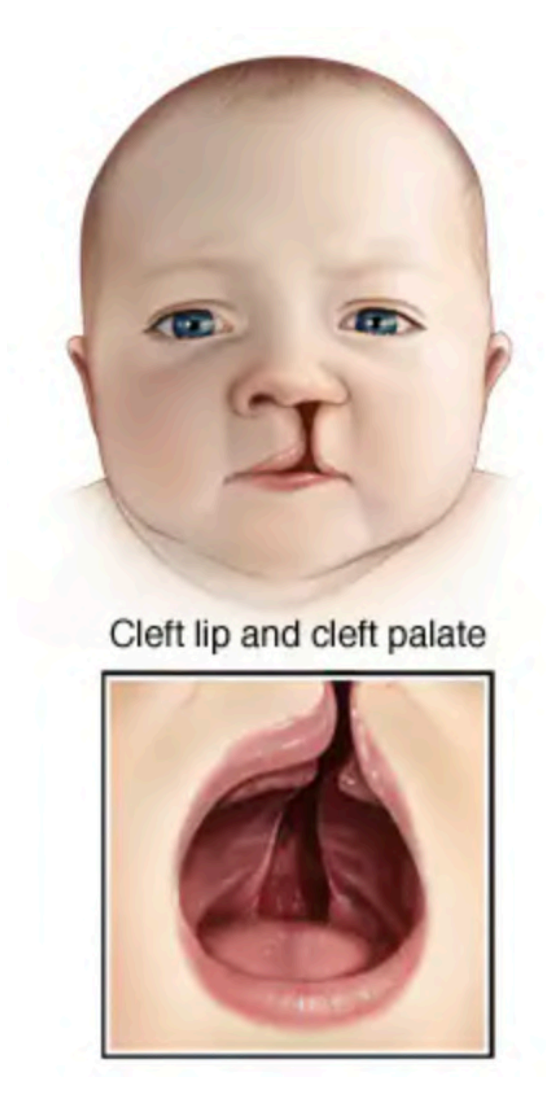


Figure 2.3 Illustration of both cleft lip and cleft palate (Adapted from [31]).

2.1.2 Epidemiology of CLP

The epidemiology of cleft lips and palate is well documented in the literature. According to the National Institute of Dental and Craniofacial Research, the annual prevalence of infants born with cleft lip with or without cleft palate is 10 in 10,000 [35]. A comprehensive systematic review and meta-analysis found that the prevalence of cleft lip and palate based on the studies reviewed in each 1000 live births was 0.45 [36]. Cleft lip and/or cleft palate is one of the most common birth defects in the U.S., affecting approximately one in 700 babies [37]. The prevalence of cleft lip and palate varies across geographic origin, racial and ethnic groups, as well as environmental exposures and socioeconomic status [38]. Parents with a family history of cleft lip or cleft palate face a higher risk of having a baby with a cleft [31]. Environmental factors such as maternal smoking and alcohol consumption have also been associated with cleft lip and palate [39]. Cleft lip and palate are a multifactorial disease caused by the interaction of genetic and environmental factors [40]. Vander Woude syndrome, which is an autosomal dominant disease, has an incidence rate of 1 in 70,000 and is closely associated with CLP or CP. This syndrome is recorded for up to 1% of all syndromic CLP cases [41].

The aetiology of non-syndromic cleft lip and palate (NS-CLP) is not well-understood, but it is known to be a multifactorial condition that involves both genetic and environmental factors during facial growth [41-44]. NS-CLP is often associated with various, bone skeletal, soft tissue, and dental deformities, such as absent or deformed teeth and skeletal abnormalities in multiple planes [45, 46]. The palatal scar tissues in NS-CLP patients can affect oral hygiene and alter the growth of the maxilla [47, 48], leading to decreased arch dimensions, particularly in the anterior region [48]. NS-CLP is a significant health anxiety that affects the life quality, status of

socioeconomic, and psychological well-being of affected individuals and their families. Although preventative measures have been focused on environmental risk factors, such as avoiding smoking and drinking during pregnancy and taking folic acid or multivitamin supplements, there is a need to identify genetic risk factors for NS-CLP as no genetic authentic counselling test has been recorded to estimate the likelihood of couples having a child with this condition [49]. Because of the cleft, the structural integrity of the palate is impaired, causing the minor part of the maxilla to rotate medio-lingually. It is believed that this rotation is brought on by the soft tissues of the face moulding around the cleft, which leads to a constricted palatal arch and a substantial anterior crossbite, with or without a posterior crossbite on the cleft side [50, 51]. The craniofacial system, maxillary morphometry, dental connections, and CLP characteristics may all be assessed in various methods. Previous studies have shown that individual CLP measures exist [52-54]. Numerous factors, including the connection between the dental arches [55], cephalograms [56-58], maxillary morphometry [59], and CBCT [60], can be used to assess the craniofacial features of CLP.

2.1.3 Treatment of CLP

Surgical interventions for CLP have evolved significantly, with modern techniques and improved anaesthesia contributing to better outcomes. Typically, lip repair occurs between 2 to 3 months of age [61], followed by palate repair at around 9 to 12 months [62]. The repair of a cleft palate requires careful repositioning of tissue and muscles to close the cleft and rebuild the roof of the mouth. Incisions are made on either side of the cleft to create flaps of skin, muscle, and intraoral tissue that are then drawn together and stitched to close the cleft and recreate typical lip and nose anatomy

[63]. Innovations like minimally invasive procedures, tissue engineering, and suturing techniques have reduced scarring and enhanced aesthetic results.

Orthodontic care plays a pivotal role in overall treatment, benefiting from digital technology and orthodontic appliances to streamline planning and progress monitoring. Patients with a cleft lip and/or palate may require multiple episodes of orthodontic treatment, e.g., before alveolar bone grafting, upper arch alignment, orthodontic camouflage, and in combination with orthognathic surgery. The duration of treatment varies depending on the type of cleft diagnosis and whether orthognathic surgery will be required. From one study, a patient with cleft lip and/or palate required an average of 44 orthodontic appointments and a mean duration of treatment of 3.4 years in order to complete their treatment [64-66].

Recent advancements in the diagnosis and treatment of cleft lip and palate (CLP) have transformed the landscape of care for affected individuals [67]. Early diagnosis remains central to a multidisciplinary approach, encompassing surgical, orthodontic, and speech therapy interventions [68]. These advancements have led to improved outcomes and quality of life for those with CLP, with ongoing research and healthcare collaboration offering the promise of further progress in the future [69]. Additionally, psychosocial support for both patients and families is now well-recognized as an essential aspect of CLP treatment, with support groups, counselling services, and online communities emerging to provide emotional assistance, share experiences, and alleviate the psychosocial burden associated with CLP [70].

2.2 Imaging Modalities for CLP

Imaging modalities are an essential component of the diagnosis and treatment of paediatric CLP. These imaging techniques allow doctors and specialists to examine

the structures of the face and mouth in detail, providing critical information that guides treatment planning. In CLP topic, we will explore the various imaging modalities used in the diagnosis and treatment of cleft lip and palate in children. We will discuss the benefits and limitations of each technique, as well as the factors that influence the choice of imaging modality in specific cases.

2.2.1 Overview of Imaging Modalities

The complex underlying causes and diverse range of symptoms associated with CLP make clinical diagnosis of this condition challenging. In this regard, diagnostic imaging modalities such as panoramic radiography, transcranial radiography, CBCT, CT, and MRI have emerged as critical tools that can aid in the accurate diagnosis of CLP [9]. In the past, conventional radiography findings were used as a basis for conservative treatment. However, with the advent of specialized imaging modalities such as CT and MRI, it has become more common to pursue a precise diagnosis to facilitate accurate and appropriate treatment. While these modalities offer increased diagnostic accuracy, their utility may be limited by factors such as cost, time, and radiation exposure. Therefore, the development of imaging guidelines could prove beneficial to guide the selection of appropriate imaging modalities for different clinical scenarios.

CBCT is a novel advancement in CT technology that is progressively being utilised for the treatment of dentofacial conditions. It is incumbent on all stakeholders to implement this technology in a responsible manner to ensure maximum diagnostic efficacy while minimising radiation exposure to patients. Despite this, the overall trend of case series within the literature implies that CBCT may offer a promising role in managing intricate defects that necessitate surgical intervention [71].

Surgical planning of CLP typically starts when the patient reaches 6 years old [19]. Multi-slice computed tomography (MSCT) is an extensively adopted technique for evaluating clefts. Although CT scans are beneficial in constructing a 3D visualisation of the patient's anatomy, the usage of ionising radiation in considerably high dosages has raised significant apprehensions regarding its utilisation in patients younger than 6 years old. Consequently, several non-systematic reviews and descriptive studies have investigated the applicability of CBCT in this context [72-78]. The acquisition of three-dimensional data allows for the assessment of bone volume required for grafting and the subsequent evaluation of bone-fill adequacy following surgical intervention [79-83].

The Guideline Development Panel of SEDENTEXCT concluded that the utilisation of CBCT for this particular application was the most straightforward to endorse, owing to the well-established utilisation of three-dimensional images and the potential for lower radiation exposure associated with CBCT [71]. It has been reported that CBCT can provide image quality as good as CT, with significantly lower dose [20].

2.2.2 Advantages and Disadvantages of Each Modality

Advancements in prenatal imaging technology have enabled the detection of cleft lip and palate (CLP), as well as associated deformities, during in-utero development [84]. Although clinical assessment is the primary means of diagnosing cleft lip, imaging remains an important tool for detecting associated anomalies, planning surgical interventions, and screening for secondary deformities. General radiography is not generally useful for diagnosing cleft lip and palate (CLP) and is therefore not typically employed for postnatal diagnosis and treatment planning

purposes [85], Nonetheless, panoramic and dental radiographs are commonly utilised for identifying dental abnormalities associated with CLP. In contrast, MRI is a valuable tool that can confirm and characterise CLP, in conjunction with prenatal ultrasonography, during prenatal diagnosis [86, 87], Postnatal MRI is generally not necessary for characterizing the cleft itself. While cleft lip and palate (CL/P) can be visualised on sagittal MRI images, coronal MRI images are better suited for depicting these abnormalities. Nevertheless, the potential risks associated with administering anaesthesia to children undergoing MRI examinations should be taken into consideration [88].

In numerous developed nations, the utilisation of X-ray technology has led to a circumstance where the cumulative and individualized yearly doses of ionising radiation as a consequence of diagnostic radiology have surpassed those originating from the previous primary source of natural background radiation [89]. Therefore, it is crucial that all radiological assessments are appropriately justified and optimised concerning radiation protection for every patient, with a special emphasis on paediatric patients. In particular, MSCT imaging for cleft lip and palate (CL/P) is highly advantageous for Visualising bone [71], Dental anatomy plays a crucial role in the repair of dentofacial anomalies, and helical CT imaging is frequently utilised for this purpose. Multiplanar reformations, utilising bone and soft-tissue algorithms, of the acquired CT images can provide an enhanced visualisation of anatomic anomalies. Furthermore, 3D reconstructions can aid in surgical planning as well as patient and family education.

CT scans may entail notably elevated radiation dosages, and roughly 7-10% of CT scans are carried out on the paediatric population [90, 91]. The organs and tissues of paediatric patients are subjected to significantly elevated absorbed doses from CT

scans, which commonly range between approximately 2 and 30 mGy for the exposed organs [88, 92].

2.3 Dose Limit and Radiation Risks

Radiation detriment encompasses the cumulative deleterious effects, quantified in terms of their severity, inflicted on a cohort and its offspring due to exposure to radiation. The magnitude of this harm is contingent on the sex and age of the affected population, thereby requiring the risk assessment to be population specific. Stochastic effects further contribute to the detriment by altering the nominal risk of cancer and heritable effects. The risk factor for the entire population, adjusted for detriment, is $5.7 \times 10^{-2} Sv^{-1}$. With regards to cancer, radiation detriment encompasses the cancer incidence rate, adjusted for its associated lethality and impact on quality of life. Table 2.1, derived from ICRP publication 103, provides a comprehensive delineation of the individual components that contribute to this aggregate value [93]. The heritable effects of dental radiography, including dental CBCT, are widely regarded as insignificant [94].

The magnitude of radiation risk is contingent upon the age of the affected individual, with younger individuals being more susceptible to its detrimental effects. Notably, in adult populations exposed to radiation doses below 50 mSv, no discernible increase in the prevalence of neoplasia has been reported. However, the risk for this age group is believed to be 2-3 times higher for foetuses, children, and adolescents [95]. The multiplication factors detailed in Table 2.2, which was derived from ICRP publication 60, ought to be employed to adjust these values [96]. Clinical procedures that entail exposure to a substantial dose of radiation, such as CT scans of the abdomen and pelvis, are associated with a dose of approximately 10 mSv. Theoretically, in a

hypothetical cohort of patients who had each undergone a single CT scan, there would be a 0.05% (1:2,000) risk of developing a fatal radiation-induced malignancy over the course of their lifetime [95]. The risk estimates provided pertain to the mean values for both sexes, with female individuals exhibiting slightly higher risks across all age groups and male individuals showing marginally lower risks.

Table 2.1 Quantifying Radiation Risks: Incorporating Detriment-Adjusted Nominal Risk Coefficients for Stochastic Effects

| | Detriment (10 ⁻² Sv ⁻¹) |
|---------------------|--|
| Cancer | 5.5 |
| Hereditable effects | 0.2 |
| Total | 5.7 |

Table 2.2 The risk estimates were adapted from the ICRP 1990 publication and are based on the multiplicative risk projection model.

| Age group (years) | Multiplication factor for risk |
|-------------------|--------------------------------|
| < 10 | × 3 |
| 10 - 20 | × 2 |
| 20 - 30 | × 1.5 |
| 30 - 50 | × 0.5 |
| 50 - 80 | × 0.3 |
| + 80 | Negligible risk |

The values presented are representative of the mean risks for both male and female individuals across different age groups.

2.4 Previous Studies on Dental CBCT

CBCT has become a vital tool in dentistry imaging, significantly transforming the field of diagnosis and treatment planning. CBCT generates highly detailed three-dimensional pictures of oral tissues while minimising the risk of radiation, making it well-suited for a range of dental applications. The use of this technology has shown to

be highly advantageous in the field of implantology, as it enables precise evaluation of the implant site and effectively minimises the occurrence of implant failures. CBCT has been extensively utilised in diverse dental disciplines, including endodontics, orthodontics, and maxillofacial surgery, to augment precision and accuracy in treatment planning. By evaluating existing studies, researchers get an essential insight about the changing field of dental imaging and its potential influence on the care of patients [97-99].

2.4.1 Overview of Studies

Our research project conducted a comprehensive review of 14 studies focused on dosimetry for CBCT, where the effective dose was calculated either by employing the ICRP publication 103 tissue weighting factors or the ICRP publication 60 tissue weighting factors, accounting for the radiosensitivity of the salivary glands and brain. The lower dose range observed for the adult phantom studies is attributed to the relatively limited range of equipment evaluated in the reviewed literature, as well as the exclusion of higher-dose equipment included in Table 2.3.

Table 2.3 Effective dose range of dental CBCT for adult phantoms: comparing large >15 cm height, medium 10 -15 cm height, and small < 10 cm height field of view exposures.

| Model type | CBCT unit type | FOV | Effective dose (µSv) | Reference |
|------------------|------------------------|--------|----------------------|-----------|
| Adult phantom | ILUMA Ultra | Large | 157, 94, 46 | [100] |
| | | Large | 84 to 194 | |
| Adult phantom | different CBCT devices | Medium | 68 to 83 | [101] |
| | | Small | 19 to 73 | |
| A dult ub aut au | : CATNC 2600 | Large | 25 to 66 | [102] |
| Adult phantom | i-CAT NG 360° | Small | 29 | [102] |
| A dult ub aut au | A lede and AVEC A | Large | 123 to 303.66 | [102] |
| Adult phantom | Alphard VEGA | Medium | 68 to 184.33 | [103] |

| | | Small | 20 to 93.67 | |
|-------------------|------------------------|--------|---------------------|---------|
| | | Large | 46 to 1073 | |
| Adult phantom | different CBCT devices | Medium | 9 to 560 | [104] |
| | | Small | 5 to 652 | |
| Adult phantom | Accuitomo 170 | Small | 111.76 to 297.97 | [105] |
| A doubt about and | 2D A amitama 170 | Medium | 240 to 250 | [106] |
| Adult phantom | 3D Accuitomo 170 | Small | 48 to 105 | [106] |
| | | Large | 174 to 2216 | |
| Adult phantom | Alphard VEGA | Medium | 289 to 366 | [107] |
| | | Small | 152 to 187 | |
| Adult phantom | CS9300 | Medium | 90.7 to 181.4 | . [100] |
| Adult phantom | RAYSCAN | Medium | 195 to 228.5 | [108] |
| | | Large | 34 | |
| Adult phantom | different CBCT devices | Medium | 88 | [109] |
| | | Small | 131 | - |

Table 2.4 presents data pertaining to the effective doses calculated for dental CBCT procedures utilising paediatric phantoms, as reported in the SEDENTEXCT project by Theodorakou et al. (2012) [110], and other relevant literature reviews.

Table 2.4 Effective dose range of dental CBCT for paediatric phantoms: comparing large >15 cm height, medium 10-15 cm height, and small <10 cm height field of view exposures.

| Model type | CBCT unit type | FOV | Effective dose (µSv) | Reference |
|---------------|------------------------|------------------|-------------------------|-----------|
| Child phantom | Dento-alveolar | Small and medium | 16-214 | [110] |
| Child phantom | Craniofacial | Large | 81-282 | [110] |
| Child phantom | different CBCT devices | Large and medium | 13 to 769 | [104] |
| | | small | 7 to 521 | |
| | | Large | 210 to 428.3 | |
| Child phantom | Alphard 3030 | Medium | 171 to 273.7 | [111] |
| | | Small | 50 to 81.46 | |
| Child phantom | Rayscan Symphony | Medium | 133 to 160.3 | [111] |

| | | Small | 141 to 154.5 | |
|---------------|--------------------------------------|---------------|-----------------|-------|
| Child phantom | Accuitomo 170 | Small | 81.54 to 126.68 | [105] |
| Cl. 11.114 | ProMax3D | Small | 88 | [110] |
| Child phantom | NewTom5G | Small | 166 to 172 | [112] |
| Child whomtom | DuaMari 2D | Small | 17.1 to 155.9 | [112] |
| Child phantom | phantom ProMax 3D Large 64.7 to 392 | 64.7 to 392.2 | [113] | |

Pauwels et al. (2012) reported on the mean proportion of organ doses that contribute to the effective dose in dental CBCT, which is illustrated in Figure 2.4 [101]. The primary contributors to the effective dose are the remainder organs, salivary glands, thyroid gland, and red bone marrow. In the case of the paediatric phantom, the contributions from the remainder organs, salivary glands, and thyroid gland are comparable, whereas for the adolescent phantom, the greatest contribution comes from the remainder organs and salivary glands, as reported by Theodorakou et al. (2012) [110].

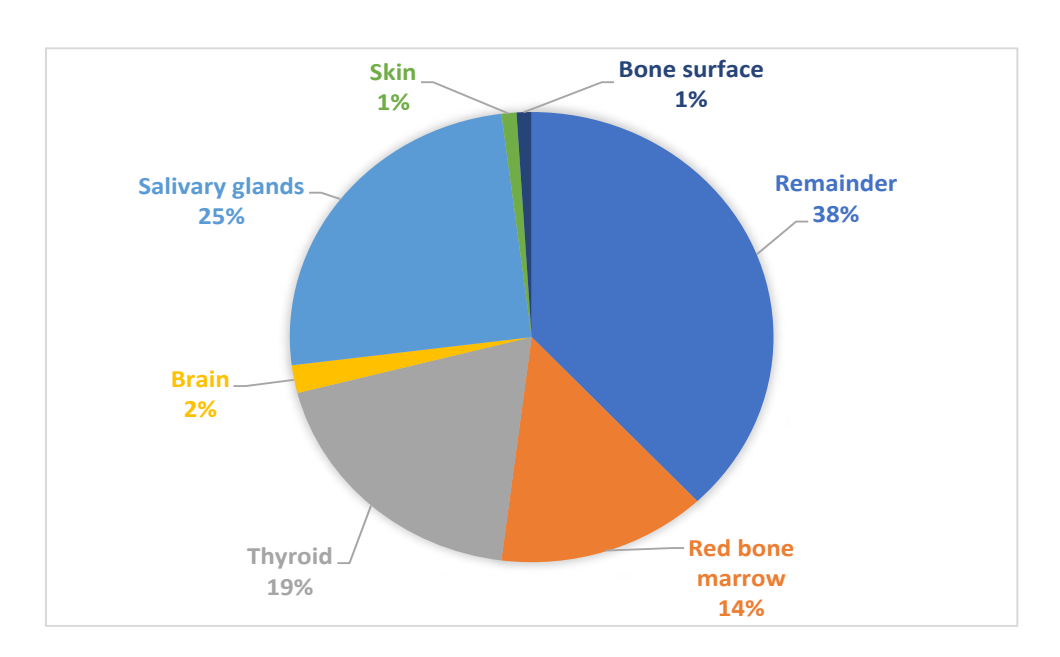


Figure 2.4 Average contribution of organ doses to effective dose calculations for CBCT.

In a recent literature review conducted by Lee et al. (2021), data was presented on the proportion of dose allocation to various tissue types, including muscle, bone, skin, soft tissue, cerebrospinal fluid, eye lens, and brain, for the CBCT imaging modality (refer to Figure 2.5). The findings indicated that a greater proportion of the total dose was administered to bone and soft tissue, whereas lower doses were distributed to the brain and cerebrospinal fluid, with percentages of 2% and 1%, respectively [114].

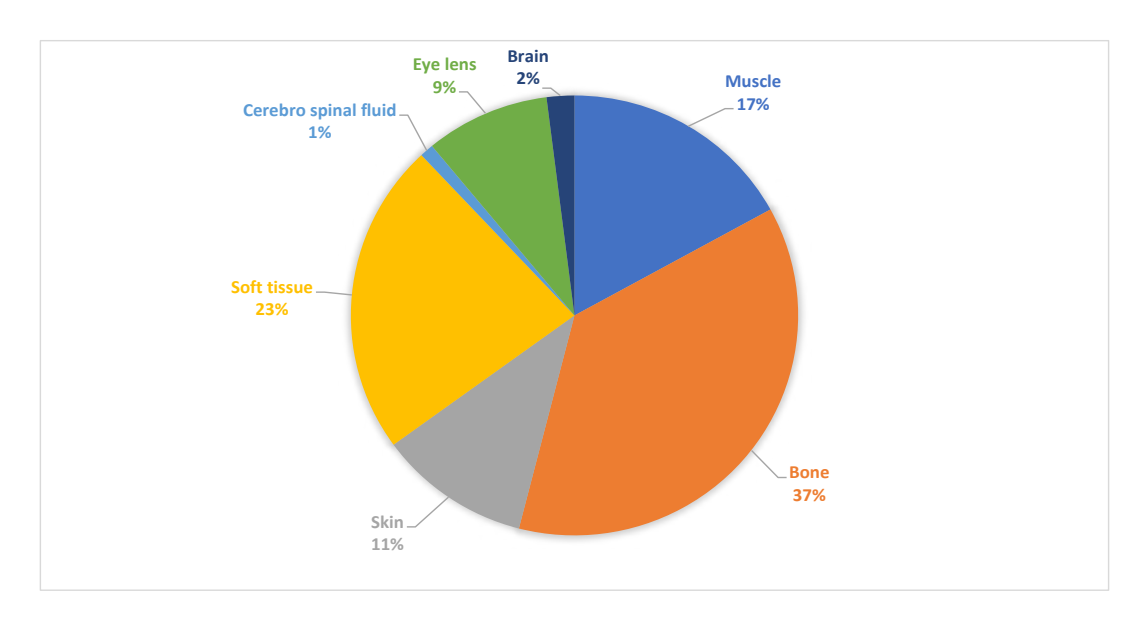


Figure 2.5 Percent fraction of radiation dose for the different tissues in the head derived from the MC-GPU simulation of the human head exposed to cone-beam computed tomography.

Table 2.5 displays a literature review comparing effective doses for conventional imaging and MSCT imaging with dental CBCT data. The studies included in this review primarily utilised thermos luminescent dosimetry (TLD) techniques with anthropomorphic phantoms. A significant degree of methodological variation was observed, particularly with respect to the phantom type used, as well as the number and positioning of TLDs. Pauwels et al. (2012), as part of the

SEDENTEXCT project, evaluated the impact of TLD number and positioning on the accuracy of dose assessments [101].

Table 2.5 Effective dose comparison among conventional dental devices

| Conventional dental devices | Effective dose (μSv) | References |
|-----------------------------|----------------------|----------------|
| Intraoral radiograph | <1.5 | [115] |
| Panoramic radiograph | 2.7 - 24.3 | [115-119] |
| Cephalometric radiograph | <6 | [115] |
| MSCT maxillo-mandibular | 280 - 1410 | [116, 119-122] |

In brief, dental CBCT typically results in greater radiation doses (and consequent risks) compared to conventional intraoral and panoramic dental radiography, yet lower doses compared to MSCT scans of the dental region. The dose level is influenced by factors such as equipment type and exposure parameters, with the field of view chosen playing a crucial role. Notably, employment of "low dose" protocols on modern MSCT equipment can significantly reduce the radiation dose. This information may be of value for researchers and practitioners seeking to optimise patient safety while obtaining necessary imaging information [120, 123-125]. The effectiveness of equipment-specific dose calculations presented in this study may quickly become obsolete, especially with the constant emergence of new equipment manufacturers. Some of the studies analysed in this review feature dental CBCT equipment that has already been replaced by newer models, although it is anticipated that current equipment will continue to be used in clinical settings for several years to come. To address the issue of ensuring current and reliable data on dental CBCT doses, computed dose simulations provide notable advantages. The SEDENTEXCT project has employed Monte Carlo modelling of computational phantoms to estimate effective doses for various dental CBCT machines and imaging protocols, eliminating the need for repeated dosimetry on anthropomorphic phantoms.